Check for updates

Archaeometry

WILEY

ORIGINAL ARTICLE OPEN ACCESS

Mortars From Punic and Hellenistic–Roman Solunto: Materials, Formulations, and Technology

G. Montana[1] | G. Polizzi[2] | C. Portale[2] | M. Gasparo Morticelli[1] | L. Randazzo[1,3]

[1]Dipartimento di Scienze della Terra e del Mare (DiSTeM), Università di Palermo, Palermo, Italy | [2]Dipartimento Culture e Società, Università di Palermo, Palermo, Italy | [3]Sezione di Palermo, Istituto Nazionale di Geofisica e Vulcanologia (INGV), Palermo, Italy

Correspondence: G. Polizzi (giovanni.polizzi02@unipa.it) | L. Randazzo (luciana.randazzo@unipa.it)

Received: 4 November 2025 | **Revised:** 18 May 2026 | **Accepted:** 6 June 2026

ABSTRACT

This study presents an archaeometric investigation of 18 hydraulic rendering and bedding mortars from Punic and Hellenistic–Roman Solunto (NW Sicily). The research aimed to characterize raw materials, reconstruct manufacturing sequences, and evaluate technological proficiency through mineralogical and petrochemical analyses. X-ray powder diffraction (XRPD), polarized light microscopy (PLM), and scanning electron microscopy with energy-dispersive spectroscopy (SEM-EDS) reveal the consistent use of magnesian aerial lime derived from local dolostones. Aggregates consist of cocciopesto (crushed pottery/brick) or local geological materials. The results clarify production techniques for hydraulic mortars made without natural pozzolans, showing that magnesium-rich binders combined with cocciopesto or dolomite yield mortars with good hydraulic performance. A key finding is the presence of hydrotalcite, a rare crystalline phase indicating advanced empirical knowledge in producing durable, water-resistant mortars. These insights enhance our understanding of ancient construction practices and support the development of compatible conservation materials.

1 | Introduction and Aims

Since Prehistory, mortars with aerial binders have demonstrated human ingenuity in transforming natural geomaterials into durable construction composites (Singer et al. 1954). In recent decades, archaeometric research on ancient and historical mortars—both in Italy and internationally—has expanded significantly, supported by increasingly refined analytical protocols (e.g., Siddall 2000; Pavía and Caro 2008; Belfiore et al. 2015, 2016; de Luca et al. 2015; Jackson et al. 2017; Lezzerini et al. 2017; Rispoli et al. 2021). Detailed characterization of raw materials not only informs restoration strategies but also provides insights into the material culture of past societies, their knowledge of local resources, and the technological skills used to enhance the performance and durability of architectural products. Reconstructing historic mortar "recipes" therefore contributes both to understanding ancient building practices and to developing compatible, sustainable conservation methods.

Despite this progress, Roman mortars from Sicily remain comparatively understudied, especially regarding their compositional and textural features, which are essential for assessing raw material provenance, technological choices, and expected performance. This contrasts with the extensive work on later historical mortars, plasters, and stuccoes from Sicily (16th–19th centuries; Montana 1997; Alaimo, di Franco, et al. 1997; Alaimo, Giarrusso, et al. 1997; Montana and Ronca 2002; Montana et al. 2008; Randazzo et al. 2015). In archaeologically significant Sicilian contexts, earlier scholarship focused mainly on stylistic aspects of wall and floor decorations (Portale et al. 2020). Only recently have archaeometric approaches gained momentum. The first such study addressed waterproof Roman mortars from the Cornelio Aqueduct at Termini Imerese (Rizzo et al. 2008), followed by analyses of bedding mortars and plasters from Palermo (Montana et al. 2016, 2018, 2019), Megara Hyblaea, and Selinunte (Bücherl et al. 2019; Mège 2021; McLennan and Keenan-Jones 2026).

G. Montana and G. Polizzi contribute equally to this work.

This is an open access article under the terms of the Creative Commons Attribution License, which permits use, distribution and reproduction in any medium, provided the original work is properly cited.

© 2026 The Author(s). *Archaeometry* published by John Wiley & Sons Ltd on behalf of University of Oxford.

FIGURE 1 | (A) Solunto: overview from the North-East; (B) Solunto: zenithal view of the public-sacred area.

The present study aims to characterize the composition and provenance of raw materials used in mortar production at the Hellenistic–Roman site of Solunto, located about 20 km east of Palermo (Figure 1A), now the focus of renewed archaeometric interest (Boese et al. 2023). It also seeks to reconstruct the manufacturing sequence, with particular attention to technological sophistication and functional performance. The resulting data may support the formulation of restoration mortars

14754754, 0, Downloaded from https://onlinelibrary.wiley.com/doi/10.1111/arcm.70185 by University Degli Studi Di Pale, Wiley Online Library on [24/06/2026]. See the Terms and Conditions (https://onlinelibrary.wiley.com/terms-and-conditions) on Wiley Online Library for rules of use; OA articles are governed by the applicable Creative Commons License

compatible with original Roman materials, which have deteriorated due to groundwater exposure and postexcavation weathering.

A previous study at Solunto was limited to a single residential context and relied mainly on indirect information about the raw materials used for lime production. Recent excavations in the northern sector (Figure 1B) now allow a more comprehensive archaeometric investigation of locally produced mortars and plasters, anchored to more precise chronological phases (Portale et al. 2023).

This study employs established mineralogical and petrographic techniques. A representative set of 18 mortar samples from Solunto was analyzed using X-ray powder diffraction (XRPD), polarized light microscopy (PLM), and scanning electron microscopy with energy-dispersive spectroscopy (SEM-EDS), providing complementary insights into mineralogical composition, microstructure, and elemental distribution.

2 | Archaeological Background

The Hellenistic–Roman town of Solunto was founded in the 4th century BC on Mount Catalfano, although recent research shows that the orthogonal urban layout visible today dates to the 3rd–2nd centuries BC (Portale et al. 2023). Although the earliest appearance of the settlement remains partly unclear, studies on the water supply system (Polizzi 2024) indicate at least two main phases of cistern construction across the site. The earliest cisterns (4th–3rd centuries BC) are small, irregular, and lined with lime-based mortars; from the late 3rd century BC onward, larger and more regular cisterns appear, coated with cocciopesto mortars. Their construction sometimes reused earlier structures, a pattern especially evident in the northern public area examined in this study (Figure S2).

More precise chronological distinctions among mortar types are now possible thanks to recent archaeometric data from a private house (Boese et al. 2023) and ongoing excavations by the University of Palermo in the sacred area and public baths (Portale et al. 2023). These investigations have identified several building phases from the late 4th century BC to the early 2nd century AD.

Phase 1 (4th–3rd centuries BC) corresponds to a predominantly Punic occupation, with dwellings beneath the theater comparable to those at Kerkouane and Selinunte (Wiegand 1997). In this area, Tusa's 1960s excavations uncovered two Punic-type bathrooms with masonry bathtubs (Polizzi 2024). In Phase 2 (late 3rd–early 2nd century BC), the street grid and insulae were reoriented and terraced. Phase 3 (mid-2nd century BC onward) saw increased building activity and monumentalization in both public and private architecture.

The first public bathing facility and its connection to the large agora cistern date to these later phases, supported by the discovery of a conduit made of Punic amphorae installed around the mid-2nd century BC (Polizzi 2024). Additional phases, identified through stratigraphy and architectural analysis, include renovations and reconfigurations of the baths (Portale et al. 2023).

The public baths (Figure S3) were built over an earlier late 4th-century BC structure of uncertain function. The complex follows a typical late Hellenistic plan, with a sequence of rooms aligned south–north. All rooms have white tessellated mosaic floors except the entrance, paved in cocciopesto. North of the building lies the service area for heating and water management; on the west side are three tanks (a–c) fed by a large public cistern, and to the east of Room 4 are the remains of a hypocaust.

Further north is a large open area with communal-sacral functions (campus? Heroon?), containing two cisterns. This sector had not been systematically studied before, apart from a preliminary overview (Greco 2020) and a chronological analysis of the cisterns (Polizzi 2024). A full study is forthcoming (Polizzi 2025). The western cistern, irregular and lined with lime plaster, belongs to Phase 1 and likely formed part of a now-lost building. The later reorganization of the insula (Phases 2 and 3) led to its destruction: An east–west wall of large limestone blocks was built within it, and at its eastern end, a large double-apsed cistern with cocciopesto lining was constructed.

3 | Geological Setting of the Area

The Hellenistic-Roman settlement of Solunto is essentially developed along the eastern slopes of Monte Catalfano. This coastal relief is considered part of the Sicilian-Maghrebide Foreland-Thrust belt, belonging to the Sagana-Belmonte Mezzagno stratigraphic-structural unit (Catalano and Montanari 1979). The investigated area is characterized by carbonate and siliceous rocks of sedimentary origin, such as calcilutite with lists and nodules of chert and dolomitized limestones (Scillato Formation); dolostones (Fanusi Formation); siliceous argillites, radiolarites, and marls (Crisanti Formation); reddish calcilutites with planktonic foraminifera, radiolarians, and sponge spicules (Caltavuturo Formation); and on the whole ranging in age from the Upper Triassic to the lower Eocene (Imerese Domain). In unconformity on these Meso-Cenozoic rocks, there are also more recent deposits, both of marine and continental origin (Calabrian-Holocene). These Quaternary deposits are composed of two main lithofacies: (1) pelitic-clayey sediments (di Stefano and Rio 1981) and (2) fossiliferous calcarenites. Both of these lithofacies have been initially attributed to the Calabrian (Sicilian) by various authors (i.e., Ruggeri and Sprovieri 1975), whereas later (di Maggio et al. 2009), the same deposits were ascribed to the Marsala Synthem (Figure S4). The Meso-Cenozoic deposits that crop out at Mount Catalfano start from the bottom with the so called “S. Elia's dolostones” (Scillato Formation, upper Trias), consisting of calcareous horizons (affected by more or less intense dolomitization which has largely obliterated both the sedimentary structures and the fossil content) and dolomitized pelagic calcareous turbidites with intercalations of breccias with light gray angular centimeter-wide elements. On the northern flank of Monte Catalfano, light gray dolostones are also observed, well stratified, with veins of greenish-yellow marly material rich in pyrite aggregates. These deposits are followed upwards by the dolomite deposit of the Fanusi Formation (upper Trias-lower Lias). Specifically, these are large banks of dolorudites and doloarenites alternating with dolomitic breccias and saccharoidal dolomites in

14754754, 0, Downloaded from https://onlinelibrary.wiley.com/doi/10.1111/arcm.70185 by University Degli Studi Di Pale, Wiley Online Library on [24/06/2026]. See the Terms and Conditions (https://onlinelibrary.wiley.com/terms-and-conditions) on Wiley Online Library for rules of use; OA articles are governed by the applicable Creative Commons License

which no traces of sedimentary structures and fossil remains are visible. The deposits of the Crisanti Formation follow in stratigraphic succession, consisting of siliceous shales and marls, well stratified in centimeter-decimetric layers, passing upwards to dark gray or black radiolarites and jaspers. On the basis of recognized rare fossils, including pelagic pelecypods, algae, and benthic foraminifera, this member is assigned to the Upper Toarcian-Early Malm. The stratigraphic section is closed by the Caltavuturo Formation (Paleocene–Upper Eocene), which is made up of reddish calcilutites and calcisiltites, foliated in places, with planktonic foraminifera, radiolarians, and sponge spicules, alternating with reddish gray marly-clayey levels, intercalated with gray bioclastic calcarenites and calcirudites with nummulites and algae.

The debris deposits on the sides of the Monte Catalfano relief are loose or weakly cemented and mainly made up of reddish-brown sandy silt including angular fragments/blocks of dolomitic and calcareous nature.

4 | Analyzed Materials and Sampling

The sampling contexts are presented in chronological order, from the oldest to the most recent. Following the principle of minimal intervention, only a limited number of significant specimens were selected after detailed macroscopic examination, ensuring representative compositional and textural characterization. Figure S1 shows the sampling points, and Table S1 provides their precise locations.

Punic bath (Polizzi 2024, 137–141): A narrow room (3.1 × 1.4 m) is likely part of a private building (4th–3rd century BC) later incorporated into the theater's substructures (Phase 1). A sample (So-M14) was taken from a small cocciopesto-coated basin on the east side.

Northern baths (Portale et al. 2021): Sample So-M13 was collected from the western wall of a public cistern built around the mid-2nd century BC (first phase of the baths, Phase 3 of the city).

Tank C (Polizzi 2024, 138): Sample So-M10 was taken from the bottom of a cocciopesto-lined tank built during the same phase, when the baths' water system was connected to the public cistern.

Trench 4 (Portale et al. 2023): Sample So-M11 derives from lime-based coatings dated to the first half–mid-2nd century BC (first phase of the baths), interpreted as remains of a floor later destroyed by the hypocaust (second phase).

Tank A (Polizzi 2024, 138): Sample So-M7 was collected from the bottom of a tank built between the 2nd and 1st century BC (second phase) during major renovations including the installation of the hypocaust.

Tank B (Polizzi 2024, 138): Samples So-M8 (bottom) and So-M9 (wall) come from a tank built at the end of the 1st century BC (third phase), after Tank A was destroyed by the construction of an apse in Room 4.

Room 2a (Polizzi 2024, 138): Samples So-M1, So-M2, and So-M3 were taken from three bedding layers beneath a whitish tessellated floor dated to the late 1st century BC (third phase). Wall coatings of cocciopesto mortar (So-M4, So-M5) belong to the same phase.

Room 3 (Polizzi 2024, 138): Sample So-M6 was collected at the base of the north wall, where a cocciopesto mortar was applied after the tessellated floor but within the same construction phase.

Trench 4 (Portale et al. 2022): Sample So-M12 was taken from deposits in a vertical drainage channel carrying water from Room 4, dated from the late 1st century BC onward.

Northern sector, Cistern No. 70 (Polizzi 2024): Sample So-M15 was collected from the eastern wall of one of the earliest cisterns (Phase 1, 4th–3rd century BC).

Northern sector, Cistern No. 71 (Polizzi 2024): Built during Phase 3 (2nd–1st century BC), this cistern has a two-layer waterproof coating: a lower lime-and-gravel layer (So-M16) and an upper cocciopesto layer (So-M17).

"Kisu" North (Polizzi 2024): Sample So-M18 comes from a quarter-circle thickening structure used to waterproof the base of the communal complex's perimeter wall, coated with cocciopesto mortar.

5 | Analytical Procedures and Methods

The mortar samples were analyzed using X-ray powder diffraction (XRPD), polarized light microscopy (PLM) on 0.03-mm thin sections, and scanning electron microscopy with energy-dispersive spectroscopy (SEM-EDS) for chemical and microstructural investigation.

XRPD focused on determining the mineralogical composition of the cryptocrystalline binder. To enrich this fraction, about 1 g of each sample was gently disaggregated to avoid breaking softer carbonate grains, and only the < 0.062 mm fraction (230-mesh) was retained. Analyses were performed with a PANalytical X'Pert Pro diffractometer (5°–60° 2θ, CuKα radiation, 40 kV, 40 mA, 2°2θ/min).

PLM observations were carried out using a Leica DLM/LSP polarizing microscope with digital camera. Aggregate abundance (area %) and aggregate-to-binder ratios were estimated semiquantitatively using comparison charts calibrated through point-counting (Matthew 1991). Additional observations on uncovered thin sections were made with a Dino-Lite digital microscope (200×, 1280 × 1024 px) under reflected and digitally polarized light.

SEM-EDS analyses were performed on selected samples representing the two main formulations (So-M4, So-M5, So-M9, So-M11, So-M12, and So-M18). Both fresh fractures (SE imaging) and polished sections (BSE imaging) were examined. Samples were carbon-coated and mounted on aluminum stubs. BSE-EDS analyses used a Thermo Scientific Phenom XL G2 SEM

14754754, 0, Downloaded from https://onlinelibrary.wiley.com/doi/10.1111/arcm.70185 by University Degli Studi Di Pale, Wiley Online Library on [24/06/2026]. See the Terms and Conditions (https://onlinelibrary.wiley.com/terms-and-conditions) on Wiley Online Library for rules of use; OA articles are governed by the applicable Creative Commons License

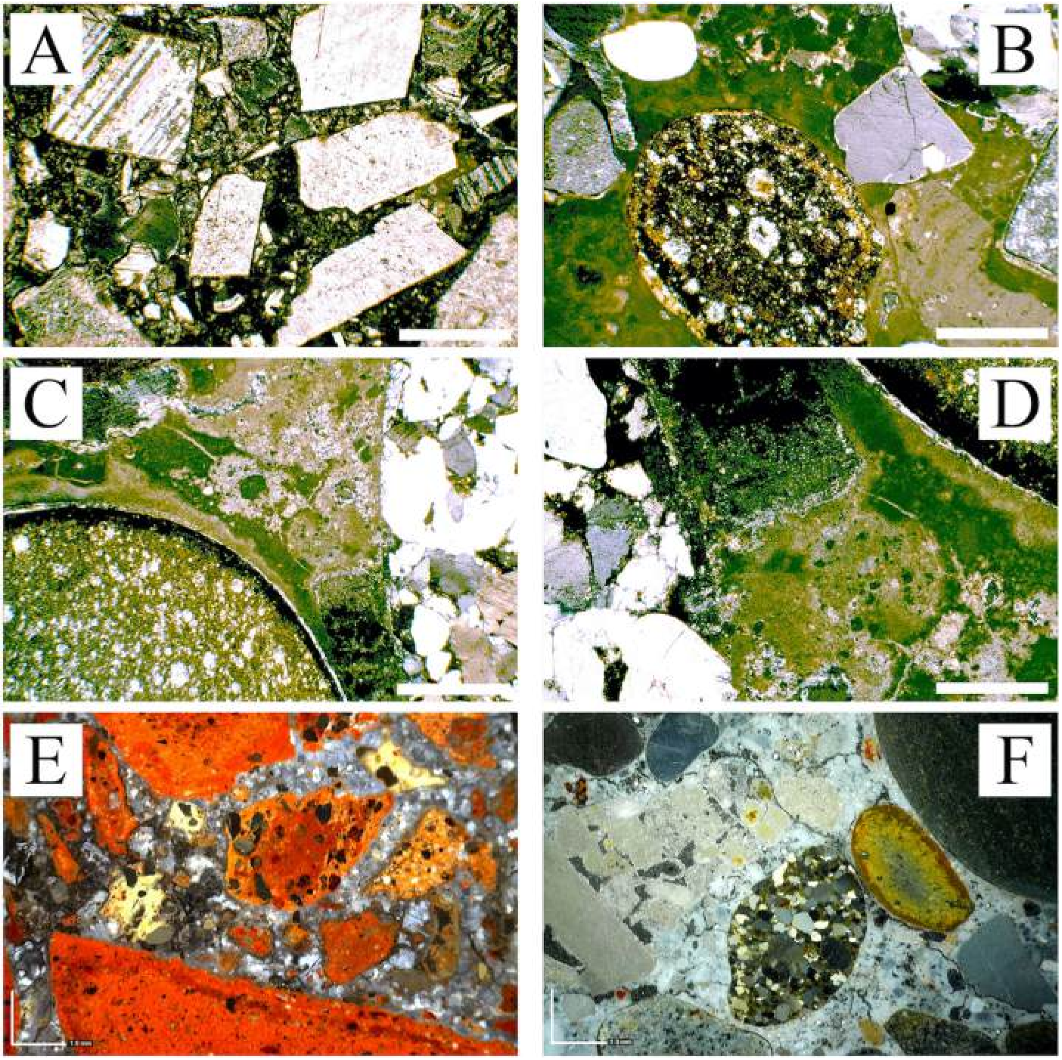

FIGURE 2 | Micrographs at polarized transmitted light microscope (A–D) and using a digital microscope (E–F): (A) Sample So-M1 (XPL, scale bar = 0.5 mm), showing abundant angular fragments of hand-crushed calcite. (B) Sample So-M2 (XPL, scale bar = 0.5 mm), characterized by subrounded to subangular grains predominantly composed of radiolarite, quartz, sandstone, and limestone. (C) Sample So-M3 (XPL, scale bar = 0.5 mm), illustrating the contact between well-rounded and coarse grains of mudstone (left) and quartzarenite (right). (D) Sample So-M3 (XPL, scale bar = 0.2 mm), showing a binder groundmass composed of nonbirefringent nanometer-sized crystals, likely magnesian phases, along with birefringent microcrystalline calcite. (E) Sample So-M7 (scale bar = 1 mm), characterized by the presence of abundant hand-crushed ceramic fragments. (F) Sample So-M11 (scale bar = 1 mm) lacks any crushed ceramic inclusions, and it is characterized by a heterogeneous aggregate comprising dolostone, quartz, quartzarenite, fossiliferous limestone, argillite, and radiolarite.

with a CeB_6 emitter, operating at 4.8–20.5 kV under low and high vacuum. SEI-EDS investigations were also conducted with a ZEISS Cross Beam UHR-SEM (HV 15 kV, 100 pA, WD 11 mm).

6 | Results

6.1 | Thin-Section Microscopy

Thin-section polarized light microscopy (PLM) was used for the petrographic classification of the mortar samples. Table S2 summarizes the main textural and compositional features of aggregates and binders. Most samples correspond to architectural linings—floor and wall coatings—associated with baths, cisterns, and water conduits. Only So-M1, So-M2, and So-M3 differ, representing the supranucleus, nucleus, and rudus of the bedding layers beneath the marble tesserae floor in Room 2a.

The supranucleus (So-M1), directly beneath the tesserae, contains a well-compacted medium-to-coarse aggregate (0.5–2 mm; ~40% area) dominated by angular calcite fragments, likely derived from locally fractured limestones or dolostones (Figure 2a). The nucleus (So-M2) and rudus (So-M3) instead include coarser alluvial sands and gravels (1–10 mm), composed of monocrystalline quartz, radiolarites, chert, sandstones, siltstones, and calcareous lithics such as mudstones, calcarenites, and bioclasts (Figure 2B,C). All three bedding layers show a heterogeneous aerial-lime binder with frequent lime lumps. The binder consists mainly of micrometric calcite crystals with variable birefringence, whereas darker, nonbirefringent areas correspond to nanometric Mg-calcite (Figure 2D).

14754754, 0, Downloaded from https://onlinelibrary.wiley.com/doi/10.1111/arcm.70185 by University Degli Studi Di Pale, Wiley Online Library on [24/06/2026]. See the Terms and Conditions (https://onlinelibrary.wiley.com/terms-and-conditions) on Wiley Online Library for rules of use; OA articles are governed by the applicable Creative Commons License

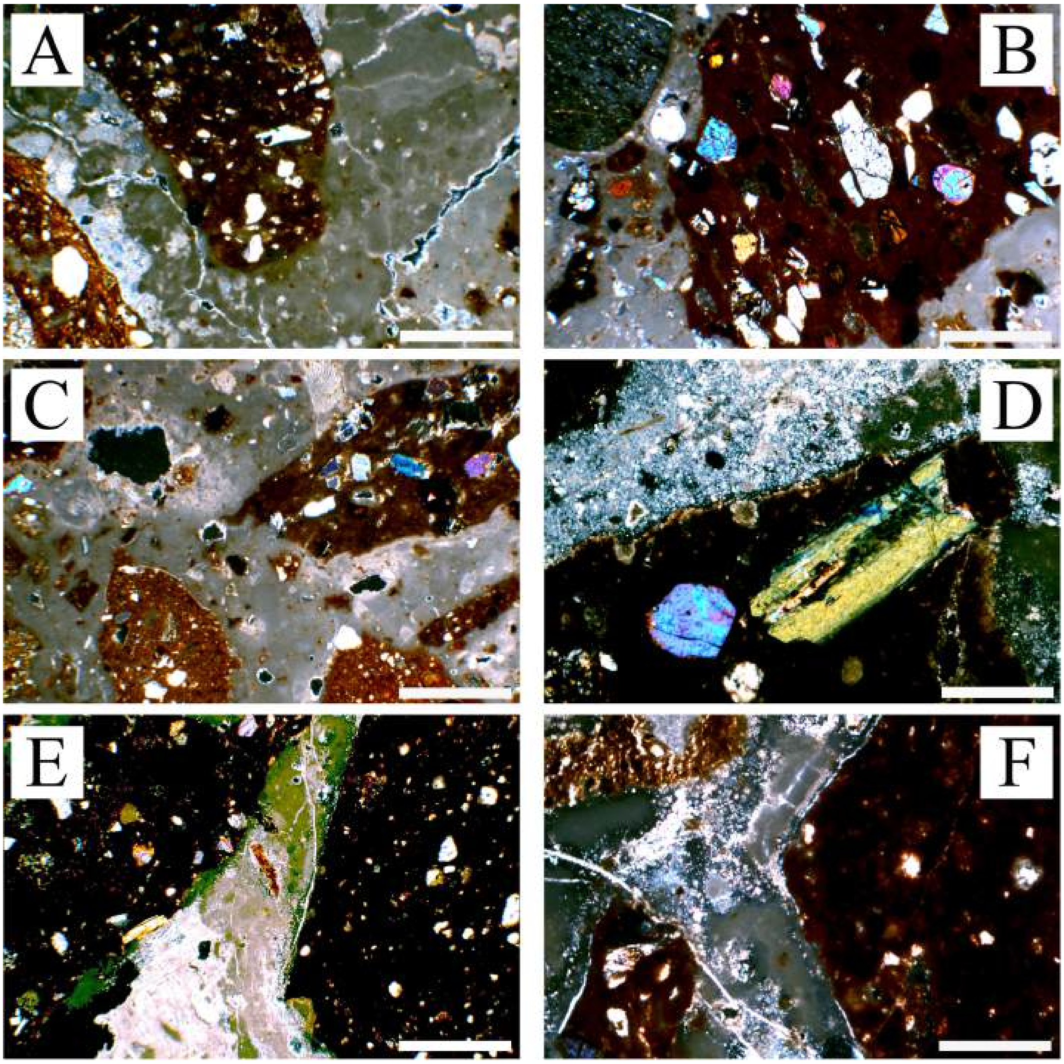

FIGURE 3 | Micrographs at polarized transmitted light microscope: (A) Sample So-M14 (XPL, scale bar = 0.5 mm), showing a millimeter-sized cocciopestofragment—locally produced—surrounded by a partially recrystallized binder matrix. (B) Sample So-M6 (XPL, scale bar = 0.5 mm), featuring a millimeter-sized cocciopesto fragment—likely originating from the Campanian–Latial Tyrrhenian coast—alongside a smaller, subrounded argillite grain (upper left). (C) Sample So-M5 (XPL, scale bar = 0.5 mm), displaying various types of crushed ceramic, primarily locally produced or imported from the Tyrrhenian coast of central Italy (see text). (D) Sample So-M9 (XPL, scale bar = 0.2 mm, showing a cocciopesto fragment)—likely originating from a transport amphora—characterized by volcanic aplastic inclusions (both minerals, i.e., clinopyroxene and lithic fragments). (E) Sample So-M8 (XPL, scale bar = 0.5 mm), binder exhibiting distinct optical activity at the contact zone between two crushed brick fragments and (F) binder showing notably varied optical activity in the contact area among multiple crushed brick fragments (XPL, scale bar = 0.2 mm).

Among the coating mortars exposed to prolonged water contact, two main formulations were identified. F1 includes abundant crushed pottery/brick fragments (cocciopesto), whereas F2 lacks cocciopesto but serves similar hydraulic functions (Figure 2E,F).

All Roman-period coating mortars (mid-2nd to 1st century BC) show high concentrations of coarse cocciopesto fragments, sometimes > 10 mm (Figure 3A,B). F1 includes So-M5, So-M6, So-M7, So-M8, So-M9, So-M10, So-M12, So-M13, and So-M17. A comparable feature appears in one Punic sample (So-M14). Besides cocciopesto, these mortars contain minor composite aggregates: monocrystalline and polycrystalline quartz, radiolarians, chert, quartz sandstones, mudstones, dolostones, limestones, calcarenites, and bioclasts—similar to those in So-M2 and So-M3. Occasional clinopyroxene grains and volcanic lithics also occur (Figure 3C,D).

All aerial-lime mortars with cocciopesto and minor alluvial sand show marked heterogeneity in optical activity (Figure 3E,F). Broad zones around ceramic fragments display very low or absent birefringence, indicating localized pozzolanic reactions and the formation of gel-like hydrated phases, the main strength-contributing components of artificial hydraulic mortars (Jackson et al. 2017; Lezzerini et al. 2017; Montana et al. 2019). Reduced optical activity also reflects the cryptocrystalline nature of these phases.

The F2 mortars (without cocciopesto) include So-M4, So-M11, So-M15 (two layers), So-M16, and So-M18. All belong to the Hellenistic–Roman period except So-M15 (Punic). So-M11 contains very coarse aggregates (2–8 mm) with roughly equal siliciclastic (quartz, chert, radiolarites, sandstones, and mudstones) and carbonate (limestone, dolostone, calcarenites, and bioclasts) components (Figure 4A), with ~60% packing density.

14754754, 0, Downloaded from https://onlinelibrary.wiley.com/doi/10.1111/arcm.70185 by University Degli Studi Di Pale, Wiley Online Library on [24/06/2026]. See the Terms and Conditions (https://onlinelibrary.wiley.com/terms-and-conditions) on Wiley Online Library for rules of use; OA articles are governed by the applicable Creative Commons License

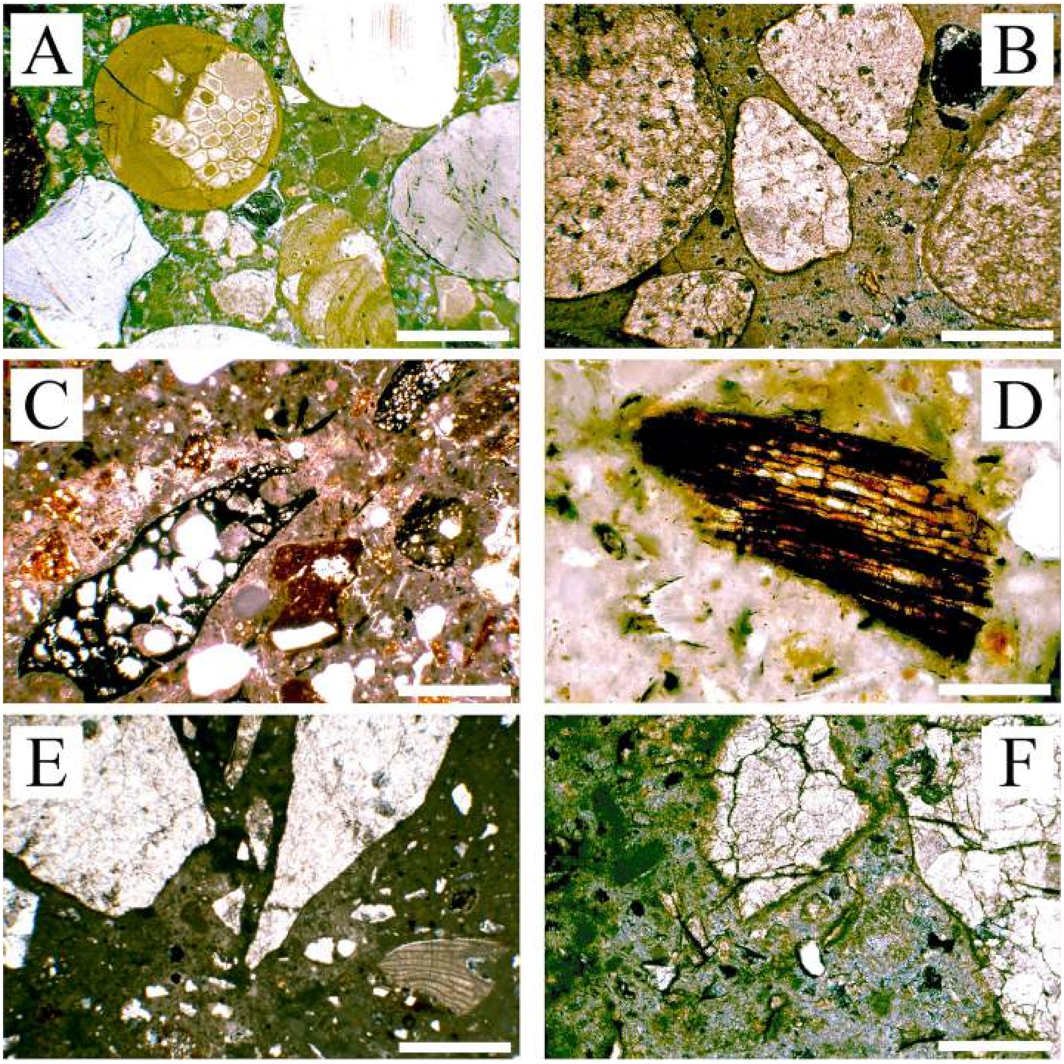

FIGURE 4 | Micrographs at polarized transmitted light microscope: (A) Sample So-M11 (XPL, scale bar = 0.5 mm), displaying subangular to rounded grains of quartz and biocalcarenite. (B) Sample So-M15 (XPL, scale bar = 0.5 mm), characterized by the presence of multiple subrounded crystalline dolostone clasts. (C) Sample So-M16 (PPL, scale bar = 0.5 mm), showing a millimeter-sized vegetal ash particle. (D) Sample So-M16 (PPL, scale bar = 0.1 mm), providing a detailed close-up of the reaction interface between the vegetal ash inclusion and adjacent binder phases. (E) Sample So-M18 (XPL, scale bar = 0.5 mm) characterized by predominantly angular dolomite rock fragments and (F) a binder exhibiting markedly varied optical activity at the contact zones among crushed dolomite fragments (XPL, scale bar = 0.2 mm).

So-M15 (Cistern 70, 4th–3rd century BC) has two layers: an inner siliciclastic-dominated layer and an outer layer dominated by angular dolomite, biocalcarenites, and pelagic limestones (Figure 4B). So-M16 closely resembles the outer layer of So-M15, with sporadic siliceous grains and a predominance of angular dolomite, biocalcarenite, and bioclasts. In So-M16 and So-M17 (the upper cocciopesto layer of Cistern 71), wood or vegetal ash occurs within the binder, likely as a calcination residue or an intentional additive to improve waterproofing (Figure 4C,D). Lime and ash also form the finishing layer of So-M7 (Tank A).

Sample So-M18 (Kisu perimeter wall, 2nd century BC) differs from the others: No cocciopesto is present, and the aggregate consists almost exclusively of freshly crushed angular dolomite fragments. Siliciclastic grains, bioclasts, and calcarenites are rare or absent (Figure 4E). Angular dolomite fragments at the binder interface, as well as rounded alluvial grains in So-M15, frequently show signs of reactivity (Figure 4F).

6.2 | X-Ray Powder Diffraction Analysis

The diffractometric analysis of the enriched binder fraction yielded several key results (Table S3). Calcite ($CaCO_3$) is the dominant crystalline phase in all samples, reflecting both binder carbonation and the presence of fine calcareous aggregates—bioclasts and limestone fragments capable of passing the 230-mesh (0.062 mm) sieve. The finest aggregate fraction, identified microscopically as coarse silt (0.04–0.06 mm), also contributes to this signal. Quartz (SiO_2), exclusively derived from the aggregate, is widespread and particularly abundant In Samples So-M4, So-M13, So-M2, So-M5, and So-M14, mostly wall coatings. Feldspars (alkali feldspar and

14754754, 0, Downloaded from https://onlinelibrary.wiley.com/doi/10.1111/arcm.70185 by University Degli Studi Di Pale, Wiley Online Library on [24/06/2026]. See the Terms and Conditions (https://onlinelibrary.wiley.com/terms-and-conditions) on Wiley Online Library for rules of use; OA articles are governed by the applicable Creative Commons License

plagioclase), detected only in trace amounts, likewise represent the finest aggregate fraction.

XRPD also clarifies the nature of the carbonate rocks used to produce aerial lime at Hellenistic–Roman Solunto. Magnesium-rich phases—magnesite ($MgCO_3$), brucite ($Mg(OH)_2$), and especially magnesian calcite ($(Ca,Mg)CO_3$)—indicate that local dolomite was the primary raw material for lime production. Quicklime (CaO) and portlandite ($Ca(OH)_2$) reflect calcination of $CaCO_3$ followed by hydration. The persistence of portlandite—unusual in ancient mortars—is likely due to restricted CO_2 diffusion; in cocciopesto mortars, pozzolanic reactions tend to retain uncarbonated portlandite (Liu et al. 2021).

Dolomite ($CaMgCO_3$) and aragonite ($CaCO_3$), detected in variable amounts, may derive either from the aggregate (dolomitic fragments and bioclasts) or from binder processes involving magnesium-rich carbonates. Although metastable under surface P–T conditions, both minerals may form in environments with thermodynamic disequilibrium—such as hypogeal settings—through percolation or biomineralization. Clay minerals occur only as minor soil-derived impurities.

The most significant XRPD finding is the widespread presence of hydrotalcite in the Solunto mortars. Hydrotalcite ($Mg_6Al_2(OH)_{16}CO_3 \cdot 4H_2O$), a layered double hydroxide structurally related to brucite, was identified in over 60% of samples, ranging from abundant to trace levels. Its diagnostic (003) reflection at ~11.3° 2θ ($d \approx 7.8$ Å; Figure S5) confirms its presence. The highest concentrations occur in mortars with aggregates dominated by dolomite fragments (So-M15 and So-M18) and in cocciopesto-rich samples (So-M13 and So-M10), suggesting multiple pathways for Mg–Al LDH formation.

6.3 | SEM-EDS Analysis

In this study, SEM-EDS analysis focused primarily on the chemical composition of the binder, complementing mineralogical data obtained through PLM and XRPD. Observations also revealed reaction interfaces between aggregate grains and the microcrystalline to cryptocrystalline binder matrix, providing insight into interaction processes at the microscale and allowing detailed examination of newly formed phases, including their size, morphology, and elemental composition.

EDS microanalysis confirms that the original binder is a magnesian aerial lime. All analyzed samples—whether or not they contain cocciopesto—show consistently high magnesium concentrations (see Figures 5 and 6). Corresponding crystalline phases include dolomite, magnesite, magnesian calcite, brucite, and hydrotalcite (Table S3). Calcium is also systematically present, associated with calcite, aragonite, portlandite, and magnesian calcite. Reaction rims at the interface between aggregates and the Mg-lime binder are more pronounced around cocciopesto fragments (Figure 5A–C) but also occur around radiolarite grains (Figure 5D).

Areas with lower Ca/Mg ratios—where magnesium phases dominate—appear darker in BSE images due to their lower backscattering coefficient. In cocciopesto mortars, these darker zones, combined with elevated Si, Al, and Mg in EDS spectra (e.g., Figure 5C), suggest the formation of noncrystalline hydrated phases such as M-A-S-H gels (Magnesia-Alumina-Silica-Hydrate) and LDH phases (Layered Double Hydroxides), likely produced through mild pozzolanic reactions (Arizzi and Cultrone 2021; Dilaria et al. 2023). These amorphous phases are not detectable by XRPD.

Hydrotalcite was also identified in Samples So-M15 and So-M18, both characterized by aggregates dominated by dolostone fragments (Tables S1 and S2). In these cases, hydrotalcite occurs in greater quantities than in cocciopesto-rich mortars. SEM observations of So-M18 clearly illustrate this: BSE imaging (Figure 6A) shows abundant magnesium compounds in the binder and a reaction rim around a large dolostone clast. Secondary electron images reveal the prismatic to lamellar morphology of hydrotalcite crystals (Figure 6B,C). EDS spot analyses confirm their composition and association with low-BSE binder regions (Figure 6D). High-magnification BSE imaging further highlights the close textural interplay between magnesium- and calcium-bearing compounds within the binder (Figure 6E).

7 | Discussion

Petrographic analyses enabled a preliminary classification of the Solunto mortar compositions into two different formulations for the same intended use (waterproof rendering): those characterized by a predominance of cocciopesto and those lacking this component. Although the distinction is readily apparent macroscopically, owing to ceramic fragments of millimeter- to centimeter-scale dimensions, detailed microscopic examination ruled out the presence of cocciopesto, even in the form of finely comminuted particles, in several of the examined mortar samples, such as Sample So-M15 (manufactured in the 4th–3rd century BC) or So-M11 (2nd century BC). Another distinctive classificatory feature, again concerning the composition of the aggregate, lies in the relative abundance of alluvial sand versus cocciopesto (see Table S2). Only a few samples (So-M16/17/18) deviate from this pattern, instead dominated by crushed dolomite fragments.

However, from a strictly chronological standpoint, no significant differences have been identified in either the recipes employed or the techniques of application. In fact, the local raw materials are represented diachronically, consistently and exclusively, by dolomite—used primarily as the calcareous rock to be calcined—and by an aggregate composed of cocciopesto and sand from the Cefalà Stream, at times accompanied by angular dolomite fragments.

On the one hand, Table S2 clearly shows that most of the mortars used to line cisterns and basins during the Hellenistic–Roman period were intentionally formulated with substantial amounts of coarsely ground ceramic fragments. These inclusions were predominantly derived from transport amphorae, either of local origin or produced along the Tyrrhenian coastal regions of Campania and Latium, as previously documented by the same authors (Bechtold et al. 2018; Montana et al. 2020, 2021). However, this trend does not apply to Samples So-M11 and So-M16, which are notable for the absence of this specific aggregate

14754754, 0, Downloaded from https://onlinelibrary.wiley.com/doi/10.1111/arcm.70185 by University Degli Studi Di Pale, Wiley Online Library on [24/06/2026]. See the Terms and Conditions (https://onlinelibrary.wiley.com/terms-and-conditions) on Wiley Online Library for rules of use; OA articles are governed by the applicable Creative Commons License

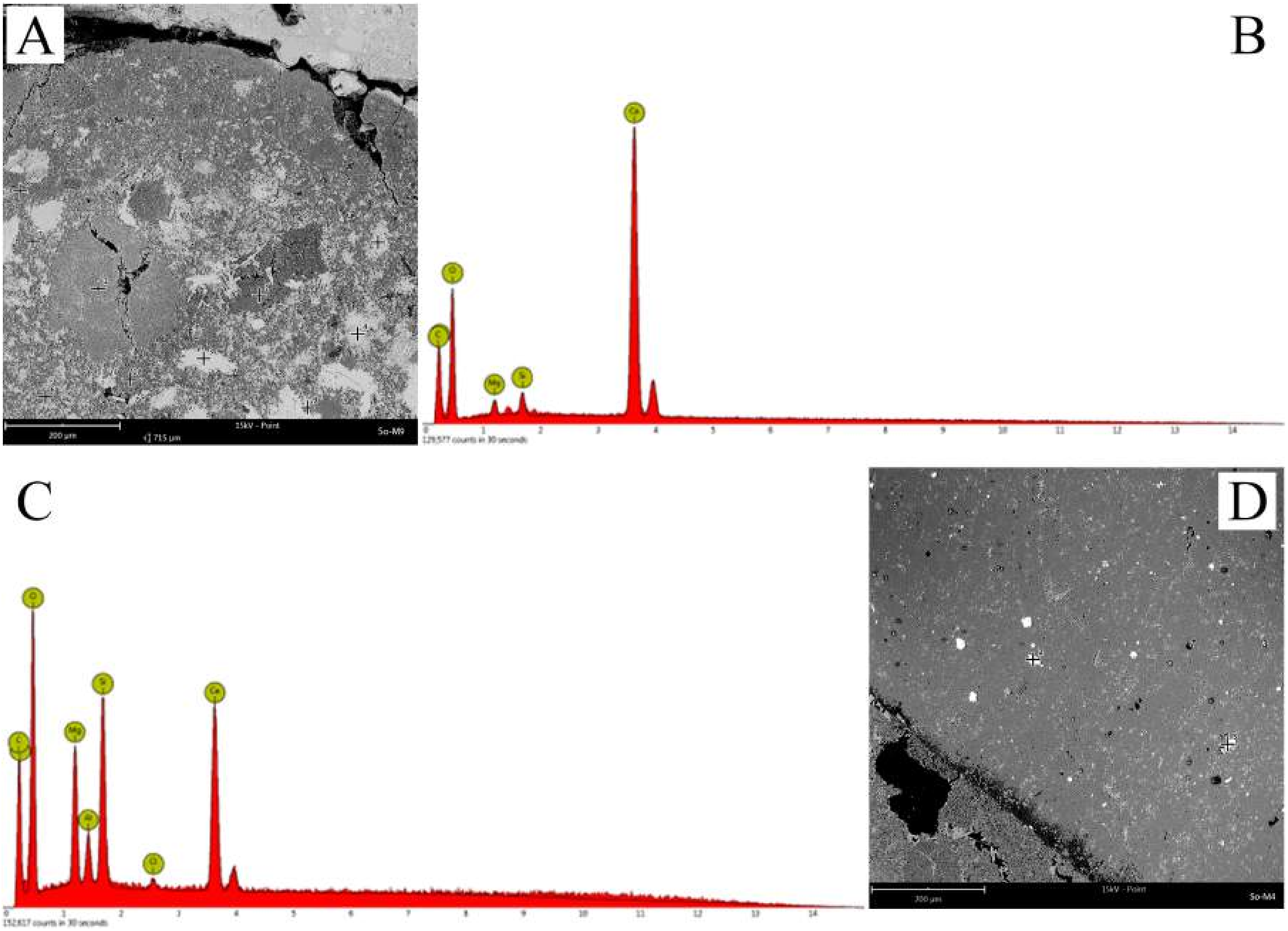

FIGURE 5 | (A) Sample So-M9, SEM image (BSE mode), showing evidence of possible reaction products (CSH and MSH) within the magnesian binder, in contact with crushed pottery fragments. Recrystallized calcite appears as large nodular formations and prismatic aggregates exhibiting a chaotic internal structure. (B) EDS spot analysis of the binder area in image (A), characterized by a higher backscattering coefficient. (C) EDS spot analysis of the binder area in image (A), characterized by a lower backscattering coefficient. (D) Sample So-M9, SEM image (BSE mode) illustrating the reaction interface between the binder matrix and a large radiolarite grain.

component. By contrast, cocciopesto was identified in Sample So-M14—attributed to Punic manufacture and dated to the 4th century BCE—thereby extending the chronological framework for its documented use within the settlement of Solunto. This finding is fully consistent with broader technological patterns: The deliberate incorporation of crushed ceramic material into mortars represents a long-standing and widely shared construction practice across the Mediterranean, attested since at least the Bronze Age (Maravelaki-Kalaitzaki et al. 2003; Theodoridou et al. 2013). Moreover, the use of cocciopesto specifically as an aggregate in hydraulic render mortars has been recently documented within Phoenician contexts—most notably at Tell el-Burak, Lebanon—dating as early as the 8th century BCE (Amicone et al. 2025). Furthermore, in the context of the settlement of Solunto, this practice could represent a significant technological achievement, most likely through the classical empirical approach, involving straightforward in situ performance evaluation. In fact, by repurposing materials from broken and functionally obsolete objects, Punic artisans were able to produce an aggregate that served as the primary component in mortars typically formulated with aerial lime binder, yielding high performance tailored to their intended hydraulic applications.

This paper does not aim to address the actual efficacy of cocciopesto in imparting hydraulic properties to aerial lime—that is, in terms of the chemical reactions leading to the formation of calcium silicates and calcium aluminate hydrates (and other aluminum and iron compounds), which renewed to be responsible for conferring hydraulic behavior to the binder. Numerous distinguished scholars have long investigated the “secrets” of these ancient mortar formulations, particularly those behind the celebrated Roman cement, which involved the use of true volcanic pozzolana (Jackson et al. 2017 and references therein; Lancaster 2019; Secco et al. 2021; Dilaria et al. 2024). In the samples analyzed at Solunto, however, pozzolana—composed of glassy scoriae, trachytoid rock fragments, alkaline feldspars, clinopyroxene, and plagioclase (see Table S2)—was identified exclusively in the first layer of Sample So-M13 and only in small quantities.

Mortars incorporating cocciopesto as an additive to aerial lime are well known for their exceptional durability, as evidenced both macroscopically and through targeted chemical and engineering analyses (Sağın et al. 2024 and references therein). However, results from the present study indicate that the

14754754, 0, Downloaded from https://onlinelibrary.wiley.com/doi/10.1111/arcm.70185 by University Degli Studi Di Pale, Wiley Online Library on [24/06/2026]. See the Terms and Conditions (https://onlinelibrary.wiley.com/terms-and-conditions) on Wiley Online Library for rules of use; OA articles are governed by the applicable Creative Commons License

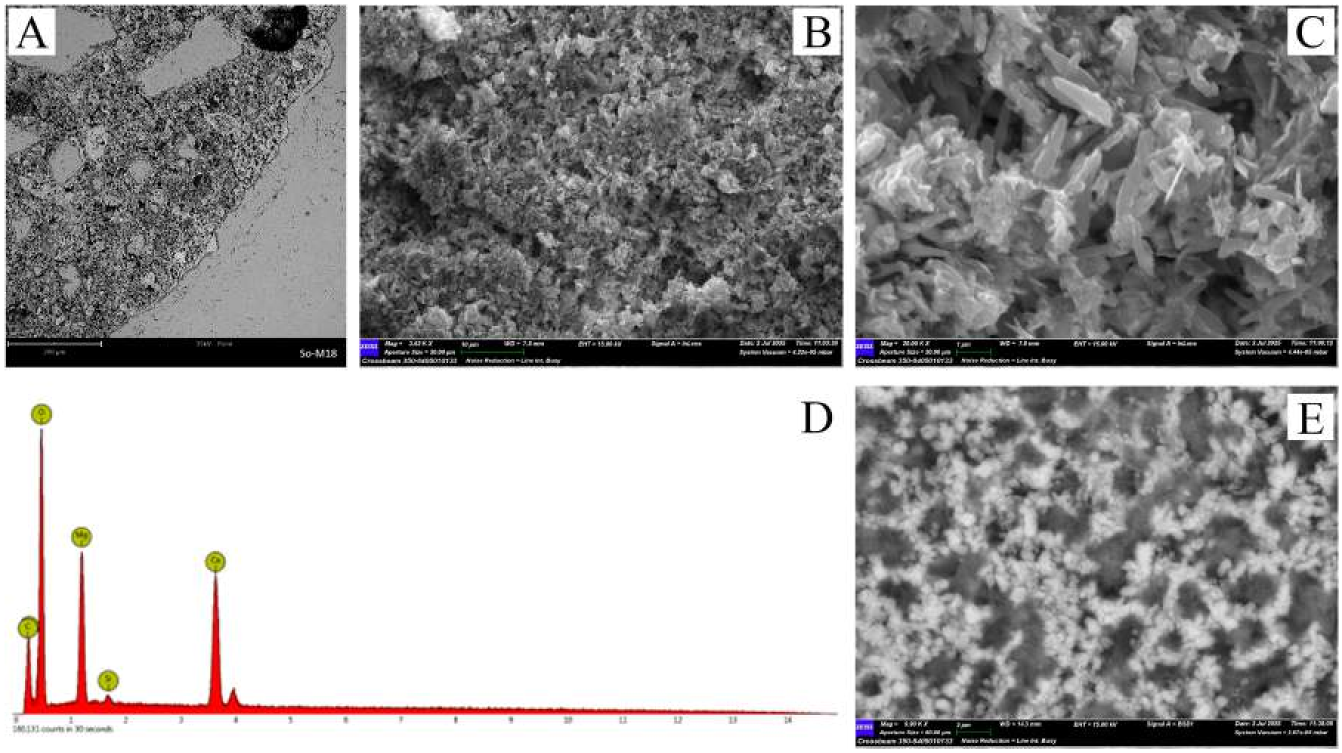

FIGURE 6 | (A) SEM image of Sample So-M18 (BSE mode), showing the interface between a large dolostone fragment and the magnesian binder. Reaction rims appear as gray-tone variations attributable to differences in backscattering coefficients, which are known to correlate directly with the mean atomic number of the involved phases. (B) SE image of Sample So-M18, highlighting areas of hydrotalcite formation and the aggregate structure. (C) SE image of Sample So-M18, providing a magnified view of the area shown in (B), with emphasis on crystal morphology. (D) EDS area analysis of the binder in Sample So-M18. (E) Backscattered electron image at high magnification showing the microtextural interplay between neo-formed phases within the binder of Sample So-M18.

chemical reactions responsible for conferring hydraulic properties are not homogeneously distributed throughout the mortar matrix. These reactions are primarily concentrated in the areas immediately surrounding ceramic fragments—manifesting as dark, optically inert regions under polarized light microscopy (Figure 3A–F) and as zones with low backscattered electron (BSE) coefficients in SEM imaging (Figure 5A).

Subsequent hardening processes result in the extensive formation of microcrystalline calcite and other newly generated compounds (Figure 6E). Thus, the overall high performance of these mortars may also be attributed to additional intrinsic factors such as low porosity and strong cohesion between binder and aggregate. These characteristics appear to mitigate the effects of compositional heterogeneity, likely stemming from the frequent sub micrometric dimensions of the newly formed phases (dark areas exhibiting minimal or absent optical activity) and the optimized compaction resulting from effective mortar application techniques. Point chemical microanalyses by SEM-EDS yield data that remain difficult to interpret unambiguously at the mineralogical level, aside from confirming the co-occurrence—primarily as aggregates of nanometric particles—of newly formed materials in both crystalline (e.g., calcium and magnesium hydroxides and anhydrous carbonates) and amorphous phases (e.g., CSH, MSH, and ASH). In this study, the interaction between cocciopesto and magnesium-rich aerial lime further complicates precise phase identification via BSE imaging and hampers the already limited correlation between chemical data and mineralogical information, due to the presence of amorphous components that do not produce X-ray diffraction (Figure 5B,C). Considering these factors, supported by experimental data, the enduring tradition of employing cocciopesto-based mortars in Solunto may be better understood as the outcome of empirically developed expertise focused on creating an efficient, low-cost coating material with satisfactory hydraulic properties—rather than a conscious effort to recycle raw materials. Further regarding the role of newly formed magnesium compounds, the presence of magnesium silicate hydrates has been documented in Late Roman mortars (4th–5th century AD) on the volcanic island of Pantelleria, Strait of Sicily (Montana et al. 2019). Reports of the presence of MSH/MASH have recently been highlighted in other Roman-era artifacts in the Mediterranean area (Alonso-Olazabal et al. 2020). Several of these mortars—formulated using local pozzolana (glassy volcanic tephra) and lime derived from calcined limestone ballast—served as cistern linings similar to those found in the much older site of Solunto, where pozzolana was not employed. Moreover, it should be noted that hydrotalcite, as well evidenced by XRPD analysis, was detected in all mortar samples formulated with cocciopesto. Therefore, it is plausible that this phase is also localized—alongside C-S-H and M-S-H—in binder areas exhibiting a relatively lower backscattering coefficient.

In the mortar manufacturing practices at the Solunto site, as clearly highlighted by petrographic analyses, the formulation of the aggregate included not only cocciopesto but also raw

14754754, 0, Downloaded from https://onlinelibrary.wiley.com/doi/10.1111/arcm.70185 by University Degli Studi Di Pale, Wiley Online Library on [24/06/2026]. See the Terms and Conditions (https://onlinelibrary.wiley.com/terms-and-conditions) on Wiley Online Library for rules of use; OA articles are governed by the applicable Creative Commons License

materials sourced from locations in close proximity to the settlement (siliceous and carbonate aggregates, sourced from the geological formations outcropping on Monte Catalfano and the immediate surroundings of the archaeological park). Among the aggregate granules in Samples So-M2, So-M3, So-M11, So-M15, So-M16, and So-M18, crystalline dolostones from the Fanusi Formation, deep sea calcilutite, chert nodules from the Scillato and Caltavuturo Formations, as well as siliceous argillite and radiolarite from the Crisanti Formation, have been readily identified and documented (Figure 4A,B,E). In addition, mono-mineralic granules of quartz and feldspars, as well as lithic fragments and bioclasts derived from the Quaternary calcarenites of the Marsala Sinthem, were also revealed as common components. In most of the examined samples, granules larger than approximately 0.5 mm—both carbonate and silicate in nature—display rounded or subrounded morphologies, which clearly indicate their origin from alluvial deposits, which are composed of eroded fragments derived from the aforementioned lithotypes. Just a few kilometers (around 2) east of the site, a stream still flows through the Vallone Cefalà, whose detrital deposits were utilized first by the Phoenicians and later by the Romans to temper clays in the production of transport amphorae and/or daily use ware as early as the 6th century BC (Montana et al. 2009; Montana and Randazzo 2015). This sand, currently retrievable at the mouth of the stream (Figure S6), despite the area's significant anthropogenic alteration, displays a lithological assortment that closely matches the previously described rock types. Moreover, quite recent archaeometric analyses of Roman-era adobe bricks from the Solunto site reveal that they were tempered with the same type of aggregate—very likely sourced from this same area (di Stefano et al. 2016). Consequently, based on the available scientific evidence, it may be reasonably concluded that the selection and procurement of sand as aggregate constituted a well-established practice in Hellenistic-Roman Solunto. Within this context, Samples So-M16 and So-M18 stand out due to their abundance of aggregate composed of crystalline dolostone and, in the case of So-M16 only, limestone. These aggregates were collected from talus deposits on the slopes of Mt. Catalfano or were artificially crushed into small angular fragments. In contrast to the variability observed in the type and relative abundance of aggregates, the binder reveals clear compositional, mineralogical, and chemical convergences. These suggest the existence of a highly standardized and long-standing production chain, passed down through centuries, consisting of the following phases: selection, procurement, preliminary processing, kiln calcination, and slaking. Indeed, both mineralogical analyses and microchemical investigations via SEM-EDS confirm the magnesian nature of the binder, which was evidently derived from the calcination of the same crystalline dolostones upon which the site of Solunto itself is founded. The concurrent presence of significant amounts of magnesite, brucite, magnesian calcite, and hydrotalcite, alongside calcite, leaves no doubt: The rock used in lime production—through both the Punic and Roman phases—was consistently the crystalline dolostone of the Fanusi Formation. Regarding the potential advantages associated with the use of magnesian lime, experimental studies indicate that they possess a suite of characteristics that render them more suitable than calcic lime for use in highly humid environments. Magnesian lime exhibits reduced values of capillarity, total porosity, lower water absorption, and enhanced durability that closely approximates the performance of an NHL 2 (Pavía and Bolton 1997; Pavía et al. 2005). The beneficial properties of magnesian lime likely account for its sustained use in Solunto over nearly four centuries, particularly in the construction of cisterns, water conduits, basins, and general masonry. Although the craftsmen lacked a scientific understanding of its composition, they relied on empirical observation to appreciate its remarkable performance, thereby perpetuating this effective and enduring construction tradition.

Another peculiarity worth noting, regarding the binder, is the presence of wood ash, limited to Samples So-M16 and So-M17 and in the finishing of Sample So-M7 (So-M7 and So-M17 have both cocciopesto aggregate). To be noted that ash-rich mortars for cistern wall coatings or floor coverings were widely documented in North Africa and Sardinia in similar periods (Davis 1981; Bonetto and Dilaria 2021; Secco et al. 2020). They were used with the aim of improving the moisture resistance performance and compressive strength, bringing it to the level of an NHL2 (Fusade et al. 2019). In our case study, the particles vary in size from a few microns to a few millimeters and are distributed in a nonhomogeneous way in the binder mass (Figure 4C,D). It seems likely that in this case the wood ash was added deliberately as an additive, rather than representing a residue resulting from the calcination process, given that it is found only in the above-mentioned samples.

Finally, it is necessary to further emphasize the significance and functional role of Mg–Al hydrotalcite. This crystalline phase was identified as a binder component in the majority of the samples. Notably, it is present in all specimens incorporating crushed ceramic (cocciopesto), though its highest concentrations were observed in those mortar samples richer in crystalline dolomite granules, such as So-M15 and So-M18. The identification of hydrotalcite represents a relatively rare occurrence of this mineralogical phase in ancient mortars (Artioli et al. 2017; Ponce-Anton et al. 2018). In natural environments, hydrotalcite typically forms through hydrothermal alterations of mafic and ultramafic magmatic rocks, such as gabbros, metagabbros, and serpentinites. Today, it is also synthesized via coprecipitation or combustion and plays a significant role in various industrial chemical applications, including heterogeneous catalysis, wastewater treatment, ion-exchange technologies, and as an additive in mortars construction materials (Lauermannová et al. 2020). In modern applications, hydrotalcite is highly valued for its ion-exchange capacity, large surface area, and stability, making it a beneficial additive in mortars and concrete, enhancing their long-term performance (durability and carbonation resistance). In this specific historical and archaeological context, the occurrence of hydrotalcite can be interpreted as a reaction product formed during the setting and hardening of lime-based materials. Its ease of formation is attributed to the structural capacity to accommodate both divalent and trivalent cations, along with a variety of anionic species. Some compounds of the double hydroxide group, namely, those based on hydrotalcite chemistry, are invariably found as products of the pozzolanic reaction between lime and clays in ancient mortars and modern binders (that serve as alternatives to Portland clinker). Thanks to its structural properties, hydrotalcite type compounds can incorporate and exchange CO_2 when exposed to the atmosphere (Artioli et al. 2017). Therefore, given its occurrence in Roman-Hellenistic mortars from Solunto—formulated with magnesian

14754754, 0, Downloaded from https://onlinelibrary.wiley.com/doi/10.1111/arcm.70185 by University Degli Studi Di Pale, Wiley Online Library on [24/06/2026]. See the Terms and Conditions (https://onlinelibrary.wiley.com/terms-and-conditions) on Wiley Online Library for rules of use; OA articles are governed by the applicable Creative Commons License

lime—it likely promotes the hydraulic reaction with reactive silicates derived from crushed ceramic aggregates.

8 | Conclusions

Mineralogical and petrographic analyses of selected Punic–Early Hellenistic and especially Hellenistic–Roman mortars from Solunto successfully met the study's objectives. A structured multi-instrumental approach enabled the identification of the following:

- The geological nature and likely provenance of raw materials used for both aggregates and binders.
- The criteria guiding raw-material selection and the technological knowledge of Soluntо's inhabitants, including changes from Punic to Roman phases.
- The performance level of the mortars in relation to formulation and function (bedding layers versus wall and floor coatings).
- The use of specific additives to enhance hydraulic behavior.
- The presence and significance of hydrotalcite, a rare crystalline phase unexpectedly widespread in both Punic and Roman mortars.

The integration of stratigraphic and analytical data confirms two main waterproofing traditions:

1. Punic period (4th–3rd century BC): lime-and-gravel mortars.
2. Roman period (late 3rd century BC–1st century AD): widespread use of cocciopesto, though isolated Punic examples also exist.

The evidence shows that Soluntine craftsmen effectively employed waterproof coatings made from cocciopesto and locally available geomaterials. Their preference for dolomitic aggregates reflects both availability and their excellent hydraulic performance, a property clearly recognized in antiquity. XRPD analyses demonstrate that most samples contain hydrotalcite, formed through reactions between local geomaterials and magnesian binders. This secondary phase likely contributed to the durability and water resistance of the earliest cistern coatings, which remain compact and efficient today. The use of cocciopesto in early bathtubs may reflect both Punic construction traditions and the esthetic appeal of its pinkish coloration.

Technological choices in waterproofing mortars reveal a deliberate selection of raw materials: crushed dolomite from the Solunto bedrock, fluvial sands from the Cefalà valley, and recycled ceramic fragments from local or imported vessels produced along the central Tyrrhenian coast (Neapolis to Albinia; Bechtold et al. 2018; Montana et al. 2020, 2021). The abundance of ceramic debris—linked to intense commercial exchanges—likely encouraged its reuse.

At Solunto, the absence of traditional pozzolanic aggregates in early mortars may be explained by the formation of hydrotalcite, whose toughness and water-repellent properties reduced the need for ash or charcoal, unlike in Punic sites such as Carthage (Davis 1981) or Nora (Bonetto and Dilaria 2021; Secco et al. 2020). Similar low ash content is noted in Punic mortars from Agrigento and Selinunte (McLennan and Keenan-Jones 2026), where local materials offered superior hydraulic qualities. Hydrotalcite likely formed through reactions between calcined dolomitic rocks ($MgO \rightarrow Mg(OH)_2$ during slaking) and aluminum hydroxides from soil impurities or minor clay additions.

Its recurring presence across periods suggests a consolidated technological tradition. However, the Hellenistic–Roman period marks a clear advancement, characterized by the systematic use of cocciopesto for waterproofing. The preference for ceramic debris from central Tyrrhenian production centers indicates a sophisticated understanding of its enhanced hydraulic behavior, linked to volcanic (pozzolanic) inclusions. Examples from the House of Harpocrates (Schön et al. 2019) and the Gymnasium (Boese et al. 2023) confirm a conscious, technically informed choice rather than opportunistic reuse.

Acknowledgments

We would like to thank the Director of the Parco Archeologico di Himera, Solunto e Monte Iato, Arch. Domenico Targia, for his strong and lasting support for research activities of the University of Palermo at Solunto. We sincerely thank the two anonymous reviewers for their helpful comments and suggestions. This paper was funded by the European Union–Next Generation EU, Mission 4 Component 2 Project SAMOTHRACE—CUP B73C22000810001. Open access publishing facilitated by Universita degli Studi di Palermo, as part of the Wiley - CRUI-CARE agreement.

Funding

This work was supported by European Union - Next Generation EU, Mission 4 Component 2 Project SAMOTHRACE - CUP B73C22000810001 (Project SAMOTHRACE - CUP B73C22000810001).

Data Availability Statement

All the information is presently accessible within the manuscript.

References

Alaimo, R., L. di Franco, V. Gagliardo Briuccia, R. Giarrusso, and G. Montana. 1997. "Plasters From the Historical Buildings of Palermo (Sicily): Raw Materials, Causes and Mechanisms of Decay." In *Proceedings of Fourth International Symposium on the Conservation of Monuments in the Mediterranean Basin*, edited by A. Moropoulou, vol. 1, 53–64. Technical Chamber of Greece.

Alaimo, R., R. Giarrusso, G. Montana, and R. Scaduto. 1997. "Composizione Delle Malte da Intonaco Utilizzate nei Prospetti Delle Ville Barocche di Bagheria." *TEMA Journal of Land Use, Mobility and Environment* 2, no. 3: 43–58.

Alonso-Olazabal, A., L. A. Ortega, M. C. Zuluaga, G. Ponce-Antón, J. Jiménez Echevarría, and C. Alonso Fernández. 2020. "Compositional Characterization and Chronology of Roman Mortars From the Archaeological Site of Arroyo de la Dehesa de Velasco (Burgo de Osma-Ciudad de Osma, Soria, Spain)." *Minerals* 10: 393.

Amicone, S., A. Orsingher, E. Cantisani, et al. 2025. "Innovation Through Recycling in Iron Age Plaster Technology at Tell el-Burak, Lebanon." *Scientific Reports* 15: 24284. https://doi.org/10.1038/s41598-025-05844-x.

14754754, 0, Downloaded from https://onlinelibrary.wiley.com/doi/10.1111/arcm.70185 by University Degli Studi Di Pale, Wiley Online Library on [24/06/2026]. See the Terms and Conditions (https://onlinelibrary.wiley.com/terms-and-conditions) on Wiley Online Library for rules of use; OA articles are governed by the applicable Creative Commons License

Arizzi, A., and G. Cultrone. 2021. “Mortars and Plasters—How To Characterise Hydraulic Mortars.” *Archaeological and Anthropological Sciences* 13, no. 9: 144.

Artioli, G., M. Secco, A. Addis, and M. Bellotto. 2017. “5. Role of Hydrotalcite-Type Layered Double Hydroxides in Delayed Pozzolanic Reactions and Their Bearing on Mortar Dating.” In *Cementitious Materials*, edited by H. Pöllmann, 147–158. De Gruyter.

Bechtold, B., G. Montana, and L. Randazzo. 2018. “Campanian Wine for Punic Sicily: Petrographic and Archaeological Studies of Graeco-Italic Amphorae From Palermo.” *Mediterranean Archaeology & Archaeometry. International Scientific Journal* 18, no. 2: 11–33. https://www.maajournal.com/index.php/maa/article/view/501/433.

Belfiore, C. M., G. V. Fichera, M. F. la Russa, et al. 2015. “A Multidisciplinary Approach for the Archaeometric Study of Pozzolanic Aggregate in Roman Mortars: The Case of Villa Dei Quintili (Rome, Italy).” *Archaeometry* 57, no. 2: 269–296. https://doi.org/10.1111/arcm.12085.

Belfiore, C. M., G. V. Fichera, G. Ortolano, A. Pezzino, R. Visalli, and L. Zappalà. 2016. “Image Processing of the Pozzolanic Reactions in Roman Mortars via X-Ray Map Analyser.” *Microchemical Journal* 125: 242–253. https://doi.org/10.1016/j.microc.2015.11.022.

Boese, B., S. Amicone, E. Cantisani, F. Schön, and C. Berthold. 2023. “Mortars in Context: An Integrated Study of Mortars and Plasters From the So-Called Ginnasio in Solunto (Sicily, Italy).” *Archaeometry* 65: 702–720. https://doi.org/10.1111/arcm.12853.

Bonetto, J., and S. Dilaria. 2021. “Circolazione di Maestranze e Saperi Costruttivi nel Mediterraneo Antico. Il Caso dei Rivestimenti in Malta Delle Cisterne Punico-Romane di Nora (Cagliari, Sardegna).” *Atlante Tematico di Topografia Antica* 31: 495–520.

Bücherl, H., O. Dally, S. Helas, and F. Schön. 2019. “Selinunt, Italien. Die Arbeiten der Jahre 2017 und 2018.” *e-Forschungsberichte des DAI* 2019, no. 2: 128–137. https://doi.org/10.34780/a41c-4c3w.

Catalano, R., and L. Montanari. 1979. “Geologia dei Monti di Trabia-Termini Imerese e dei Monti Sicani Orientali (Fogli Bagheria e Termini Imerese, Sicilia Centro Settentrionale).” *Rendiconti Accademia Scienze FF. MM. Della Società Nazionale Scienze Lettere e Arti* 46, no. 4: 1–27.

Davis, L. H. 1981. “A Note on Some Cistern Mortars Found at Carthage.” In *Excavations at Carthage 1977*, 43–49. Kelsey Museum, University of Michigan.

de Luca, R., D. Miriello, A. Pecci, et al. 2015. “Archaeometric Study of Mortars From the Garum Shop at Pompeii, Campania, Italy.” *Geoarchaeology* 30: 330–351. https://doi.org/10.1002/gea.21515.

di Maggio, C., M. Agate, A. Contino, L. Basilone, and R. Catalano. 2009. “Unconformity-Bounded Stratigraphic Units of Quaternary Deposits Mapped for the CARG Project in Northern and Western Sicily [Unità a Limiti Inconformi Utilizzate Per la Cartografia dei Depositi Quaternari Nei Fogli CARG Della Sicilia Nordoccidentale].” *Alpine And Mediterranean Quaternary* 22, no. 2: 345–364.

di Stefano, C., R. Giarrusso, G. Montana, and A. Mulone. 2016. “Caratterizzazione di Mattoni in Terra Cruda di età Ellenistico-Romana Dall'area Archeologica di Solunto (Palermo) e di Provini Ottenuti con Materie Prime Locali.” In *Materiali Antichi per un Futuro Sostenibile. Atti del Workshop (Palermo, Palazzo Montalbo, 11/12/2015)*, edited by E. Cilia Platamone and R. Not, 79–88. Dipartimento dei Beni Culturali e della Identità Siciliana, Centro Regionale per la Progettazione e il Restauro.

di Stefano, E., and D. Rio. 1981. “Biostratigrafia a Nannofossili e Biocronologia del Siciliano Nella Località Tipo di Ficarazzi (Palermo-Sicilia).” *Acta Naturalia Dell'Ateneo Parmense* 17: 97–111.

Dilaria, S., G. Ricci, M. Secco, et al. 2024. “Vitruvian Binders in Venice: First Evidence of Phlegraean Pozzolans in an Underwater Roman Construction in the Venice Lagoon.” *PLoS ONE* 19, no. 11: e0313917.

Dilaria, S., M. Secco, J. Bonetto, G. Ricci, and G. Artioli. 2023. “Making Ancient Mortars Hydraulic. How to Parametrize Type and Crystallinity of Reaction Products in Different Recipes.” In *Historic Mortars International Conference*. RILEM Bookseries, vol. 42, 36–52. Springer.

Fusade, L., H. Viles, C. Wood, and C. Burns. 2019. “The Effect on Wood Ash on the Properties and Durability of Lime Mortars for Repointing Damp Historic Buildings.” *Construction and Building Materials* 212: 500–513. https://doi.org/10.1016/j.conbuildmat.2019.03.326.

Greco, C. 2020. “A Proposito del Ginnasio di Solunto.” In *Studi in Onore di Stefano Vassallo*, edited by M. Chiovaro and R. Sapia, 114–119. Assessorato dei Beni Culturali e dell'Identità siciliana.

Jackson, M. D., S. R. Mulcahy, H. Chen, et al. 2017. “Phillipsite and Al-Tobermorite Mineral Cements Produced Through Low-Temperature Water-Rock Reactions in Roman Marine Concrete.” *American Mineralogist* 102, no. 7: 1435–1450. https://doi.org/10.2138/am-2017-5993CCBY.

Lancaster, L. C. 2019. “Pozzolans in Mortar in the Roman Empire.” In *Mortiers et hydraulique en Méditerranée*, edited by I. F. Ortega and S. Bouffier. Presses Universitaires de Provence.

Lauermannová, A. M., I. Paterová, J. Patera, K. Skrbek, O. Jankovsky, and V. Bartunek. 2020. “Hydrotalcites in Construction Materials.” *Applied Sciences* 10: 7989. https://doi.org/10.3390/app10227989.

Lezzerini, M., M. Ramacciotti, F. Cantini, et al. 2017. “Archaeometric Study of Natural Hydraulic Mortars: The Case of the Late Roman Villa dell'Oratorio (Florence, Italy).” *Archaeological and Anthropological Sciences* 9: 603–615. https://doi.org/10.1007/s12520-016-0404-2.

Liu, W., Y. Li, L. Tang, and F. Xing. 2021. “Modelling Analysis of Chloride Redistribution in Sea-Sand Concrete Exposed to Atmospheric Environment.” *Construction and Building Materials* 274: 121962. https://doi.org/10.1016/j.conbuildmat.2020.121962.

Maravelaki-Kalaitzaki, P., A. Bakolas, and A. Moropoulou. 2003. “Physico-Chemical Study of Cretan Ancient Mortars.” *Cement and Concrete Research* 33: 651–661.

Matthew, A. J. 1991. “Spots Before the Eyes: New Comparison Charts for Visual Percentage Estimation in Archaeological Material.” In *Recent Developments in Ceramic Petrology*, edited by A. Middleton and I. Freestone, vol. 81, 399–409. British Museum Occasional Paper.

McLennan, R., and D. Keenan-Jones. 2026. “Connectivity and Change in the Waterproofing Technology of Ancient Sicily: Evidence From Selinunte and Agrigento.” *Archaeological and Anthropological Sciences* 18: 32. https://doi.org/10.1007/s12520-025-02364-7.

Mège, F. 2021. “Ancient Concretes and Mortars of Selinous: Preliminary Results of the Project CaF “Concretes as Floors”.” *Archäologischer Anzeiger* 2021, no. 2: 1–15. https://doi.org/10.34780/4739-8g64.

Montana, G. 1997. “Materiali e Tecnologia di Produzione Della Calce a Palermo nei Secoli Passati: Implicazioni nel Restauro dell'Architettura Monumentale Barocca e Neoclassica.” *Mineralogica et Petrographica Acta* 40: 373–383.

Montana, G., A. Corretti, and R. Giarrusso. 2008. “Caratterizzazione Mineralogico-Petrografica Delle Malte in Opera nel Castello di Calatamauro a Contessa Entellina (Sicilia occidentale).” In *Atti del V Congresso Nazionale di Archeometria*, edited by A. Gueli, 329–342. Morrone Editore.

Montana, G., I. Iliopoulos, V. Tardo, and C. Greco. 2009. “Petrographic and Geochemical Characterization of Archaic-Hellenistic Tableware Production at Solunto, Sicily.” *Geoarchaeology* 24, no. 1: 86–110. https://doi.org/10.1002/gea.20251.

Montana, G., and L. Randazzo. 2015. “La Caratterizzazione Delle Produzioni di Anfore Punico-Siciliane.” *Carthage Studies* 9: 118–146.

Montana, G., L. Randazzo, D. Barca, and M. Carroll. 2021. “Archaeometric Analysis of Building Ceramics and ‘Dolia Defossa’ From the Roman Imperial Estate of Vagnari (Gravina in Puglia, Italy).”

14754754, 0, Downloaded from https://onlinelibrary.wiley.com/doi/10.1111/arcm.70185 by University Degli Studi Di Pale, Wiley Online Library on [24/06/2026]. See the Terms and Conditions (https://onlinelibrary.wiley.com/terms-and-conditions) on Wiley Online Library for rules of use; OA articles are governed by the applicable Creative Commons License

Journal of Archaeological Science: Reports 38: 103057. https://doi.org/10.1016/j.jasrep.2021.103057.

Montana, G., L. Randazzo, and B. Becthold. 2020. "The Beginning of Western Greek Amphorae Production in Western Sicily: Archaeometric and Archaeological Studies on 6th–5th Centuries BCE Amphorae Manufactured in Himera." *Minerals* 10, no. 9: 762. https://doi.org/10.3390/min10090762.

Montana, G., L. Randazzo, M. R. Cerniglia, C. Aleo Nero, and F. Spatafora. 2016. "Production Technology of Early-Hellenistic Lime-Based Mortars Originating From a Punic-Roman Residential Area in Palermo (Sicily)." *International Journal of Conservation Science* 7: 797–812.

Montana, G., L. Randazzo, S. Vassallo, and F. Udine. 2018. "The Mosaic of the Frigidarium of "Villa Bonanno" in Palermo: Mineralogical and Petrographic Analyses for In Situ Conservation and Restoration Interventions." *Mediterranean Archaeology and Archaeometry* 18, no. 5: 95–107.

Montana, G., L. Randazzo, C. Ventura-Bordenca, R. Baldassari, and A. M. Polito. 2019. "The Production Cycle of Lime-Based Plasters in the Late Roman Settlement of Scauri, on the Island of Pantelleria, Italy." *Geoarchaeology* 34, no. 6: 631–647. https://doi.org/10.1002/gea.21697.

Montana, G., and F. Ronca. 2002. "The "Recipe" of the Stucco Sculptures of Giacomo Serpotta." *Journal of Cultural Heritage* 3, no. 2: 133–144. https://doi.org/10.1016/S1296-2074(02)01169-X.

Pavía, S., and J. Bolton. 1997. "Laboratory Studies of the Interaction Between Bedding/Pointing Mortar and Building Stones." *International Journal for Restoration of Buildings and Monuments* 3, no. 3: 253–268.

Pavía, S., and S. Caro. 2008. "An Investigation of Roman Mortar Technology Through the Petrographic Analysis of Archaeological Material." *Construction and Building Materials* 22: 1807–1811. https://doi.org/10.1016/j.conbuildmat.2007.05.003.

Pavía, S., B. Fitzgerald, and R. Howard. 2005. "Evaluation of Properties of Magnesian Lime Mortar." In *Structural Studies, Repair and Maintenance of Heritage Architecture IX*. Transaction on the Built Environment, edited by C. A. Brebbia and A. Torpiano, vol. 83, 375–384. WIT Press.

Polizzi, G. 2024. *Solonte et l'Eau. L'Exploitation des Ressources en eau Dans la Cité Antique de Solonte*. Palermo University Press.

Polizzi, V. 2025. "Il Complesso a Ovest della Casa Delle Ghirlande a Solunto." *Thiasos* 14: 353–372. http://thiasos.eu/wp-content/uploads/2025/08/20-2025-Polizzi-V.pdf.

Ponce-Anton, G., L. A. Ortega, M. Cruz Zuluaga, A. Alonzo-Olazabal, and J. L. Solaun. 2018. "Hydrotalcite and Hydrocalumite in Mortar Binders from the Medieval Castel of Portilla (Alava, Noth Spain): Accurate Mineralogical Control to Achieve More Reliable Chronological Ages." *Minerals* 8, no. 8: 326. https://doi.org/10.3390/min8080326.

Portale, E. C., G. Milazzo, and G. Montali. 2020. "Nuovi Dati Sulle Decorazioni Parietali di Solunto." In *Animum Pictura Pascit (Verg., Aen. i, 464). Abitare con le Pitture nel Mediterraneo Antico. Atti Delle Giornate Gregoriane XII Edizione (Agrigento, 29 Novembre–1 Dicembre 2019)*, edited by V. Caminneci, M. C. Parello, and M. S. Rizzo, 157–172. AnteQuem.

Portale, E. C., G. Montali, M. Limoncelli, G. Polizzi, L. Fazio, and D. Giuliano. 2021. "Nuove ricerche a Solunto (2021)." *Mare Internum* 13: 115–154.

Portale, E. C., G. Montali, G. Polizzi, M. Limoncelli, and M. Cangemi. 2022. "Ricerche a Solunto (2022)." *Mare Internum* 14: 161–185.

Portale, E. C., G. Montali, L. Sole, G. Polizzi, M. Limoncelli, and L. Schepis. 2023. "Solunto 2023: Scavi e Ricerche Nell'area Urbana." *Mare Internum* 15: 117–135.

Randazzo, L., G. Montana, R. Alduina, E. Tsantini, and B. Salemi. 2015. "Flos Tectorii Degradation of Mortars: An Example of Synergistic Action Between Soluble Salts and Biodeteriogens." *Journal of Cultural Heritage* 16, no. 6: 838–847. https://doi.org/10.1016/j.culher.2015.04.002.

Rispoli, C., R. Esposito, L. Guerriero, and P. Cappelletti. 2021. "Ancient Roman Mortars From Villa del Capo di Sorrento: A Multi-Analytical Approach to Define Microstructural and Compositional Features." *Minerals* 11, no. 5: 469. https://doi.org/10.3390/min11050469.

Rizzo, G., L. Ercoli, B. Megna, and M. Parlapiano. 2008. "Characterization of Mortars From Ancient and Traditional Water Supply Systems in Sicily." *Journal of Thermal Analysis and Calorimetry* 92: 323–330.

Ruggeri, G., and R. Sprovieri. 1975. "La Definizione Dello Strato Tipo del Piano Siciliano e le sue Conseguenze." *Rivista Mineraria Siciliana* 151-153: 8–14.

Sağın, E. U., H. E. Duran, and H. Böke. 2024. "Archaeometric Study of Roman Bricks and Cocciopesto Aggregates From the Ancient City of Nysa, Western Anatolia." *Journal of Archaeological Science: Reports* 57: 104594. https://doi.org/10.1016/j.jasrep.2024.104594.

Schön, F., S. Amicone, C. Berthold, B. Boese, and T. P. König. 2019. "Archaeometric Data for the Urbanistic Development of Solunto (Sicily/Italy) - The Casa Di Arpocrate. First Results of the Tübingen-Mortar-Project." In *Cityscapes of Hellenistic Sicily: A Reassessment*, edited by G. Adornato and M. Trümper. Proceedings of the Conference Held in Berlin, 15–18 June 2017. Edizioni Quasar.

Secco, M., Y. Asscher, G. Ricci, et al. 2021. "Cementation Processes of Roman Pozzolanic Binders From Caesarea Maritima (Israel)." *Construction and Building Materials* 355: 129128.

Secco, M., S. Dilaria, J. Bonetto, et al. 2020. "Technological Transfers in the Mediterranean on the Verge of the Romanization: Insights From the Waterproofing Renders of Nora (Sardinia, Italy)." *Journal of Cultural Heritage* 44: 63–82.

Siddall, R. 2000. "The Use of Volcaniclastic Material in Roman Hydraulic Concretes: A Brief Review." *Geological Society, London, Special Publications* 171: 339–344. https://doi.org/10.1144/gsl.sp.2000.171.01.24.

Singer, C., E. J. Holmyard, and A. R. Hall. 1954. *A History of Technology, Volume I.: From Early Times to Fall of Ancient Empire*, 882. Clarendon Press.

Theodoridou, M., I. Ioannou, and M. Philokyprou. 2013. "New Evidence of Early Use of Artificial Pozzolanic Material in Mortars." *Journal of Archaeological Science* 40: 3263–3269.

Wiegand, A. 1997. *Das Theater von Solunt. Ein besonderer Skenetyp des Späthellenismus auf Sizilien*. Verlag Philipp von Zabern.

Supporting Information

Additional supporting information can be found online in the Supporting Information section. **Figure S1:** Plan of the northern sector of Solunto (GIS elab. G. Polizzi). **Figure S2:** Cistern built between the 4th/3rd century obliterated by subsequent structures. **Figure S3:** Plan of the North Baths. 1: entrance to the Baths from the agora; 2a and 2b: service or changing rooms; 3: *apodyterium*-massage rooms; 4: *calidarium* (GIS elab. G. Polizzi). **Figure S4:** Geological map depicting the exposed formations and lithological units in the vicinity of the Solunto archaeological site. **Figure S5:** XRPD spectrum of Sample So-M18 reveals the diagnostic (003) reflection of Mg–Al hydrotalcite at approximately 11.3° 2θ (Cu Kα radiation), corresponding to a d-spacing of ~7.8 Å. **Figure S6:** Alluvial sand collected at the mouth of the stream that flows through Vallone Cefalà, in proximity to the ancient settlement of Solunto. **Table S1:** Details of sampling points and general information concerning the analysed samples. **Table S2:** Petrographic features of plaster samples after thin-section observations. **Table S3:** Semiquantitative mineralogical composition after XRPD analysis.

14754754, 0, Downloaded from https://onlinelibrary.wiley.com/doi/10.1111/arcm.70185 by University Degli Studi Di Pale, Wiley Online Library on [24/06/2026]. See the Terms and Conditions (https://onlinelibrary.wiley.com/terms-and-conditions) on Wiley Online Library for rules of use; OA articles are governed by the applicable Creative Commons License